

Article

Development of Indium Titanium Zinc Oxide Thin Films Used as Sensing Layer in Gas Sensor Applications

Sheng-Po Chang ^{1,*} , Ren-Hao Yang ² and Chih-Hung Lin ³¹ Department of Photonics, National Cheng Kung University, Tainan 701, Taiwan² Institute of Microelectronics & Department of Electrical Engineering, National Cheng Kung University, Tainan 701, Taiwan; roy810426@gmail.com³ Taiwan Semiconductor Research Institute, Tainan 701, Taiwan; y9008230@gmail.com

* Correspondence: changsp@mail.ncku.edu.tw

Abstract: InTiZnO gas sensors with different oxygen ratios were fabricated by RF sputtering at room temperature. The sensing responses for five different gases, including ethanol, isopropanol (IPA), acetone (ACE), CO, and SO₂, were reported. The InTiZnO gas sensor with the MSM (metal–semiconductor–metal) structure generated a higher sensing response when the O₂/Ar ratio was increased to 10%. It also revealed high selectivity among these gases and good repeatability. Moreover, the UV light-activated InTiZnO gas sensors were also studied, which could reduce the operating temperature from 300 °C to 150 °C and did not seem to damage the sensing film, demonstrating long-term stability. The high response and selectivity revealed that InTiZnO thin films possess high potential to be applied in gas sensing technology.

Keywords: indium–titanium–zinc oxide; gas sensor; co-sputter; UV light

Citation: Chang, S.-P.; Yang, R.-H.; Lin, C.-H. Development of Indium Titanium Zinc Oxide Thin Films Used as Sensing Layer in Gas Sensor Applications. *Coatings* **2021**, *11*, 807. <https://doi.org/10.3390/coatings11070807>

Academic Editors: María Dolores Fernández Ramos and Octavian Buiu

Received: 15 April 2021
Accepted: 1 July 2021
Published: 3 July 2021

Publisher's Note: MDPI stays neutral with regard to jurisdictional claims in published maps and institutional affiliations.



Copyright: © 2021 by the authors. Licensee MDPI, Basel, Switzerland. This article is an open access article distributed under the terms and conditions of the Creative Commons Attribution (CC BY) license (<https://creativecommons.org/licenses/by/4.0/>).

1. Introduction

The metal oxide semiconductor gas sensor has attracted much attention for environmental monitoring, the detection of harmful gases, and even noninvasive breath diagnosis. Compared with other materials, metal oxide gas sensors have been widely investigated because of their high sensitivity, low cost, and simplicity in production [1]. Research indicates that the sensitivity and the reversible reaction of the gas reacting with the material surface could be affected significantly by some key factors, such as the chemical composition, nature of the materials, temperature, illumination, and defects in sensing layers [2,3]. To date, gas sensors based on different kinds of metal oxide materials, including SnO₂ [4], ZnO [5], WO₃ [6], TiO₂ [7], ITO [8], and CuO [9], have been studied widely.

These metal oxide thin films are known for their wide bandgap, high resistivity, and excellent optical transmittance (>80%) in the visible region [10–12]. Among these materials, InTiZnO has been studied because of its wide bandgap of 4 eV [13], which is wider than that of typical metal oxide thin films. Because TiO₂ is a well-known photocatalyst, a InTiZnO gas sensor illuminated at different operating temperatures for comparative purposes was studied. However, the high energy consumption due to the high operating temperature was a challenge in the development of these portable products. The high operating temperature may also result in reliability problems. Several methods have been proposed to reduce the device temperature, such as microelectromechanical system (MEMS) fabrication [14] and the use of ultraviolet (UV) lighting [15–19].

In this study, not only the organic vapors such as ethanol (C₂H₅OH), acetone (C₃H₆O), and isopropanol (C₃H₈O) but also inorganic vapors such as carbon monoxide (CO) and sulfur dioxide (SO₂) are detected by a InTiZnO gas sensor at 300 °C. We use films with different oxygen flow ratios to measure the response of each gas. To overcome the energy consumption issue, the gas sensor, which is activated by UV light, is also discussed.

2. Materials and Methods

The following procedures were used to fabricate the InTiZnO gas sensor. Figure 1 shows the structure of the device. Quartz substrates were cleaned with acetone, isopropyl alcohol, and deionized (DI) water sequentially every five minutes in an ultrasonicator. After rinsing, they were dried with nitrogen. Next, we used an RF sputter (Cluster Multi-Chambers Sputter System, Kao Duen Technology Corporation, Taiwan) to grow the film at room temperature. The 200 nm InTiZnO thin film was deposited on quartz substrates with various oxygen flow ratios by sputtering an InTiZnO target (In:Ti:Zn = 99:1:99 in molar ratio). Before the deposition, the sputtering chamber was pumped down at a base pressure of under 5×10^{-6} Torr. The RF power was fixed at 80 W, and the substrates were rotated at a speed of 20 rpm. The oxygen/argon flow ratio was manipulated. The total flow of gas was 50 sccm, with an argon flow of 50 to 45 sccm and an oxygen flow of 0 to 5 sccm. Sample A to Sample D had flow ratios of 0% (50 sccm Ar), 6% (3 sccm O₂, 47 sccm Ar), 8% (4 sccm O₂, 46 sccm Ar), and 10% (5 sccm O₂, 45 sccm Ar), respectively. Lastly, Ni/Au (30/70 nm) metal contacts as electrodes were deposited on the quartz substrates through an interdigitated shadow mask by thermal evaporation. Figure 2a shows the XRD (Nanostar U System, Bruker AXS GmbH, Karlsruhe, Germany) spectrum of the InTiZnO thin films. The curve shows that the thin films were all amorphous, without annealing and with no obvious diffraction peaks. The peaks in the spectrum were at 21.5° and 33°, which were attributed to the quartz substrate. Figure 2b shows TEM (JEOL JEM-2100F Ultrahigh Resolution Transmission Electron Microscope, Tokyo, Japan) cross-section images of the InTiZnO thin films. In the image, the film can be clearly divided into different layers. According to the TEM cross-section results, it is confirmed that the entire thickness of the device was approximately consistent with our complete fabrication process parameters.

The sample was placed on the heating platform. The heating platform shown in Figure 1 heats up and maintains the temperature of the sensor. And we confirm the temperature of the platform with a thermocouple instrument. And then, we measured the I-V characteristics in the air from interdigitated electrodes of the sensing film. Subsequently, we injected the analyte into the sealed chamber through a microliter syringe. Then, we continuously measured the current of the sensor with a Keithley 4200 (Model 4200A-SCS Parameter Analyzer, Keithley Instruments Cleveland, OH, USA) semiconductor parameter analyzer after it was stabilized in the presence of analyte gases.

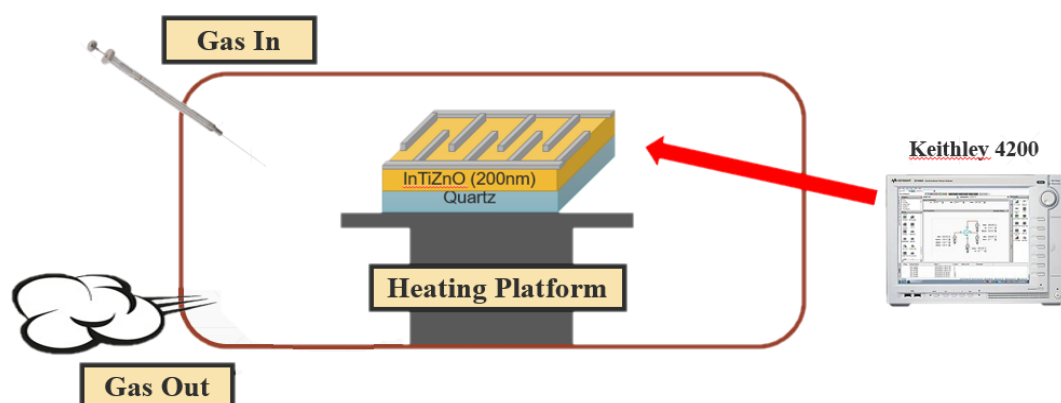


Figure 1. MSM structure of InTiZnO gas sensor and the measurement environment of the gas sensor.

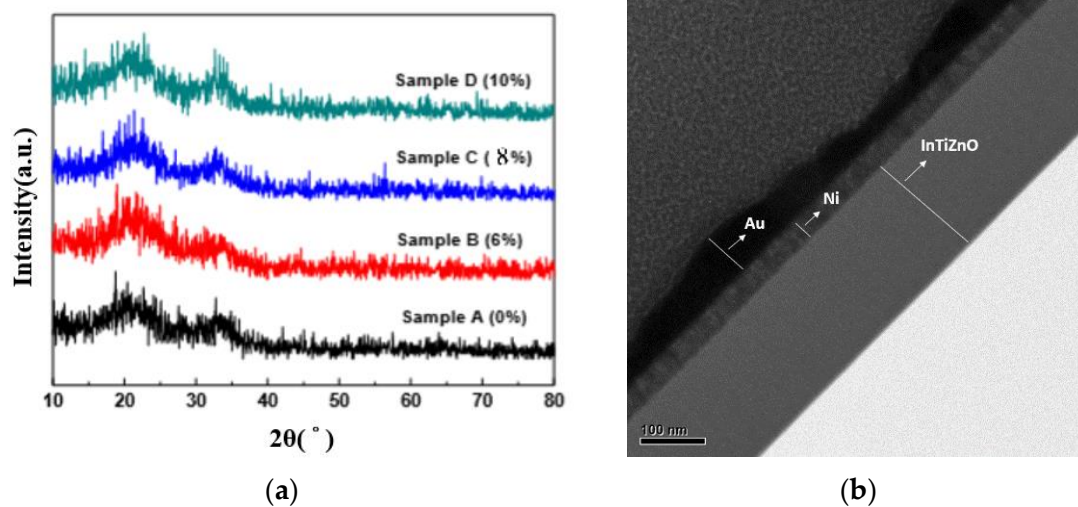
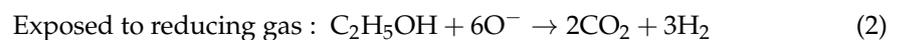
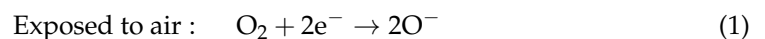


Figure 2. (a) XRD spectra of as-deposited InTiZnO thin film with various oxygen flow ratios (b) cross-section TEM image of InTiZnO film.

3. Results

As shown in Figure 3, ethanol was injected into the chamber and then we opened the cavity to diffuse the alcohol back into the atmosphere under the condition of continuous current conduction. A 5V bias was applied to the sensor across the top interdigitated electrodes during the measurement. We then observed the current change. In the presence of the reducing gas, the measured current increased when the test gas was injected. Through the measurement, we could see that the InTiZnO film was the N-type. When we exposed the N-type semiconductor to a reducing gas (C_2H_5OH), due to the exchange of electrons between the ionosorbed species and sensing film, the resistance of the InTiZnO film decreased, as shown in Equation (2). Figure 3a–c show the current transients for Samples A to C when injecting the ethanol gas. Figure 3d shows a comparison of the responsivity of each sensor under different ethanol concentrations. The response could be calculated from Equation (3) below, and the value was 320%, 663%, and 1001% for Samples A to C, respectively. As the oxygen flow increased, the response to ethanol became higher. In addition, Sample C had an excellent response to ethanol compared to gas sensors of other materials [20–22].



$$\text{Response} = [(I_{\text{gas}} - I_{\text{air}}) / I_{\text{air}}] \times 100\% \quad (3)$$

The relation between oxygen flow ratio and gas sensing responsivity could be attributed to the surface morphology and defect theory [1]. Figure 4 shows the AFM measurement (D5000, Veeco, New York, USA) of the InTiZnO thin film [23]. The increasing root mean square (RMS) value of surface roughness from 1.1 nm to 1.4 nm was attributed to the enhancement of the O_2/Ar ratio. The excess oxygen ions bombarded the surface and affected the surface roughness. With the increasing oxygen ratio, more oxygen ions bombarded the films, bringing about a rising RMS value of roughness. The responsivity increased due to their larger surface-to-volume ratio [24].

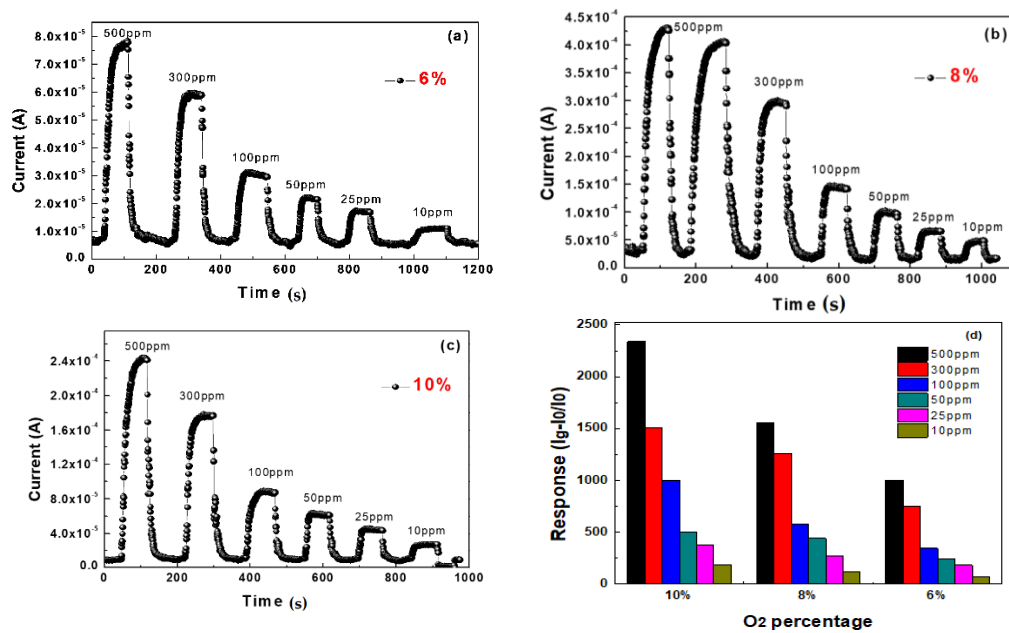


Figure 3. Sensing transients to ethanol for samples with (a) 6%, (b) 8%, and (c) 10% oxygen flow ratio at 300°C, respectively. (d) Variation in sensitivity with ethanol gas concentration.

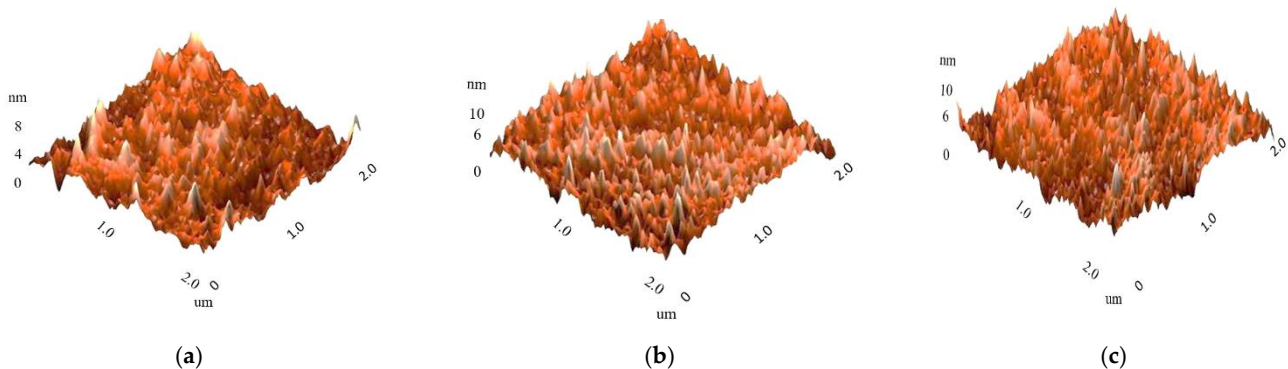


Figure 4. AFM images of InTiZnO thin film of (a) Sample B (RMS value: 1.1 nm), (b) Sample C (RMS value: 1.2 nm), (c) Sample D (RMS value: 1.4 nm).

On the other hand, Figure 5 shows the X-ray photoelectron spectroscopy (XPS) (Phi 5000 VersaProbe, Ulvac-Phi. Inc., Kanagawa, Japan) results. Figure 5a–d are the XPS spectra of O1s for the InTiZnO film grown with various oxygen flow ratios. The spectra were de-convoluted in two peaks: one peak (OI) occurred at 529.6 eV, corresponding to O atom binding in bulk InTiZnO, and the other peak (OII) was located at around 531.3 eV and attributed to oxygen deficiencies, such as oxygen vacancies and oxygen interstitials, in InTiZnO. It can be clearly seen that the ratio of OII decreased from 78.8% to 57.7% as the oxygen flow ratio increased from 0% to 10%. It could be elucidated that when the oxygen flow ratio decreased, the number of oxygen vacancies in the crystal increased, and the chemisorptive oxygen ion traps rather recombined back to the oxygen vacancies in the bulk phase. This caused the reduction of surface traps and then lowered the responsivity. Figure 6 shows the response mechanisms of a chemisorptive sensor. We use surface chemical adsorption and defect theory as an explanation. The oxygen ion trap originally adsorbed on the surface at a high temperature tended to compound the oxygen defects in the sensing film. When the oxygen flow rate during deposition was higher, the amount of oxygen vacancies was filled and reduce. Then, when we measured the samples at high temperatures, the composite trap was reduced, and more traps remained on the surface to react with the gas, so the response was higher.

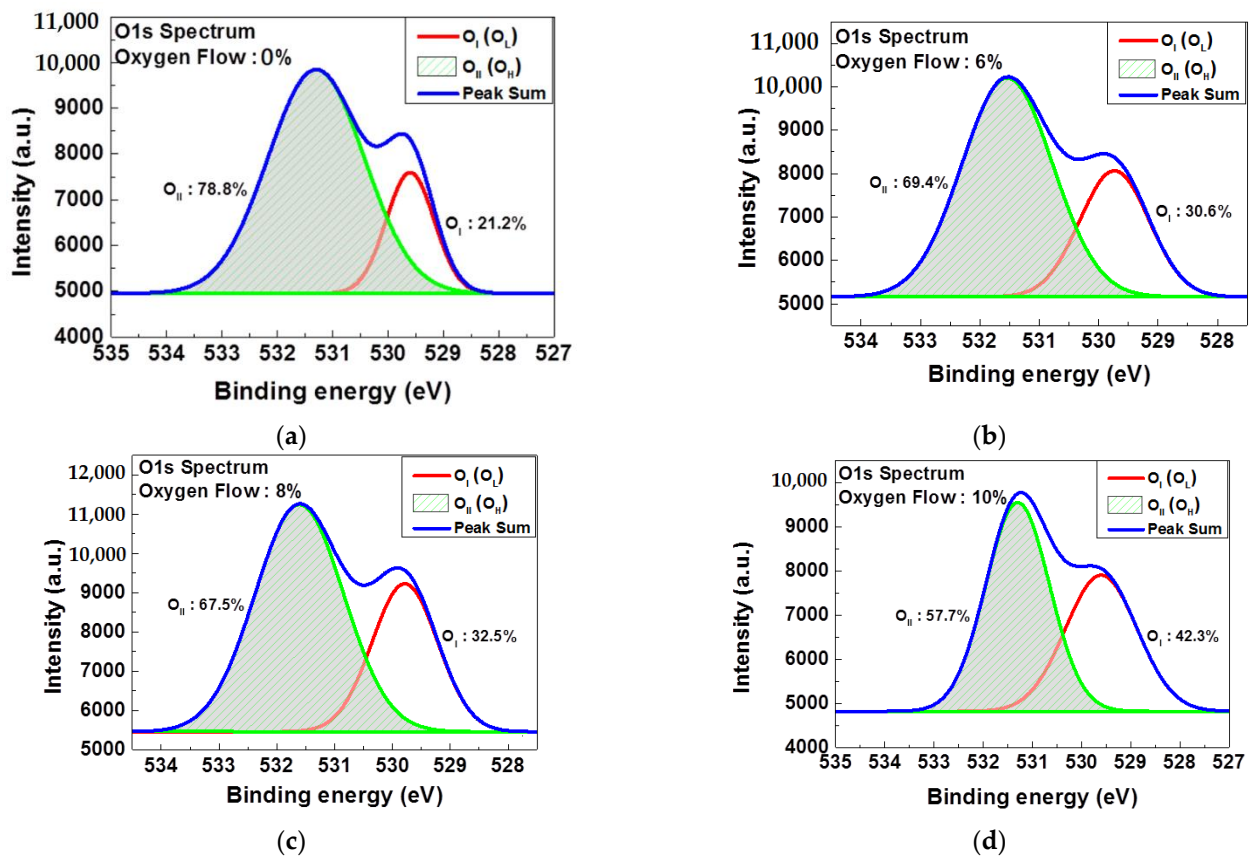


Figure 5. XPS O1s spectra of InTiZnO thin film with various oxygen flow ratios: (a) 0%, (b) 6%, (c) 8%, (d) 10%.

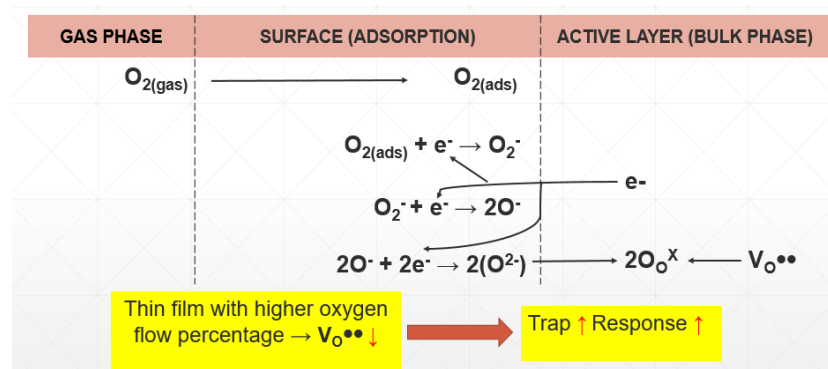


Figure 6. Response mechanisms of chemisorptive sensor.

When the sensor was exposed to IPA, acetone, and CO at 300 °C, the sensing response of the device was observed and is shown in Figure 7a–c. The device with a 10% oxygen flow ratio had higher responsivity than the other conditions. We can see that the trend is the same as in Figure 3. The responses for different gases under a 100 ppm concentration exposed to 10%, 8%, and 6% samples are shown in Figure 7d. When comparing the responsivity of different oxygen ratios for ethanol, IPA, ACE, and CO, we found that Device D not only had the highest responsivity but also had the highest selection to ethanol among these gases. This confirmed that the InTiZnO sensor also had good sensitivity with an appropriate oxygen flow ratio during the sputtering.

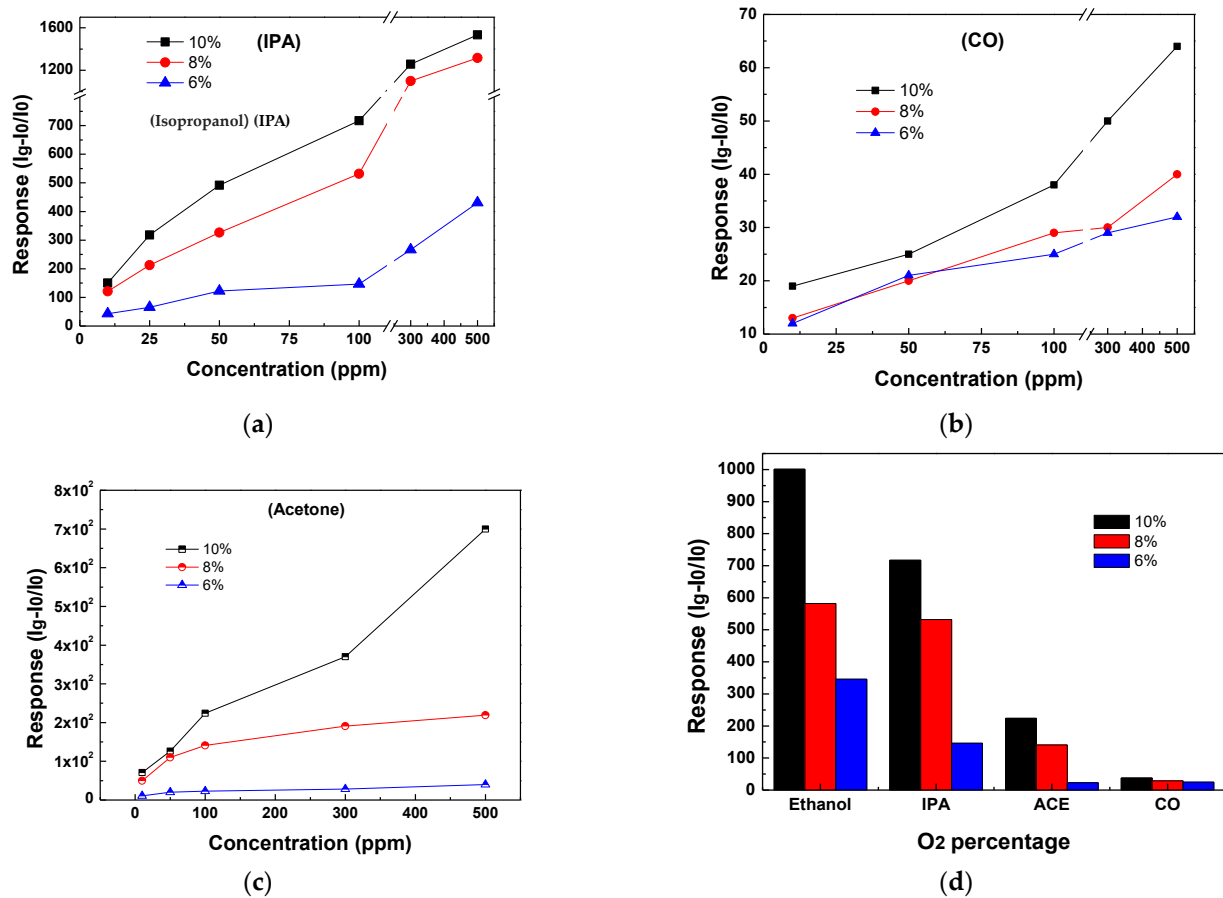


Figure 7. Comparative sensing behavior (300 °C) in response to different oxygen flow percentages as a function of (a) isopropanol (IPA), (b) CO, and (c) acetone concentration. (d) Responses of 100 ppm different gases exposed to 10%, 8%, 6% samples.

The gas sensing property toward sulfur dioxide (SO₂) was also considered. The injection of gas was performed from a fixed concentration to a fixed volume, and then it was converted into ppm because of the different test chambers. Figure 8a–c show the response to SO₂. The current increased because SO₂ was a strongly reducing gas, but it did not recover to the initial value after the gas injection. It took a long time but still could not reach a saturated state. The graph in Figure 8d shows the responsivity of the sensors. The experiment revealed that the responsivity was reduced with a higher SO₂ concentration, showing the opposite trend compared with the other gases in this study. This phenomenon was attributed to the corrosivity and saturated adsorption of SO₂. Table 1 shows the exact responsivity evaluated in Figure 8d.

Figure 9 shows that Device D was treated with UV light irradiation under 100 ppm of ethanol gas and different temperatures. The wavelength of UV light was 345 nm and the power was 6 watts. The current transient was affected by UV radiation, and the process could be divided into two stages. In the beginning, the current increased rapidly because of the electron–hole pairs induced by UV irradiation and then reached saturation. From Figure 9a, it can be seen that the sensitivity was 412% when we injected 100 ppm ethanol at 250 °C without UV treatment, and the current raised again after the sample was irradiated by UV light. When the current was saturated, the same concentration of ethanol was injected and we observed the same gas-sensing behavior, but the responsivity dropped from 412% to 58%.

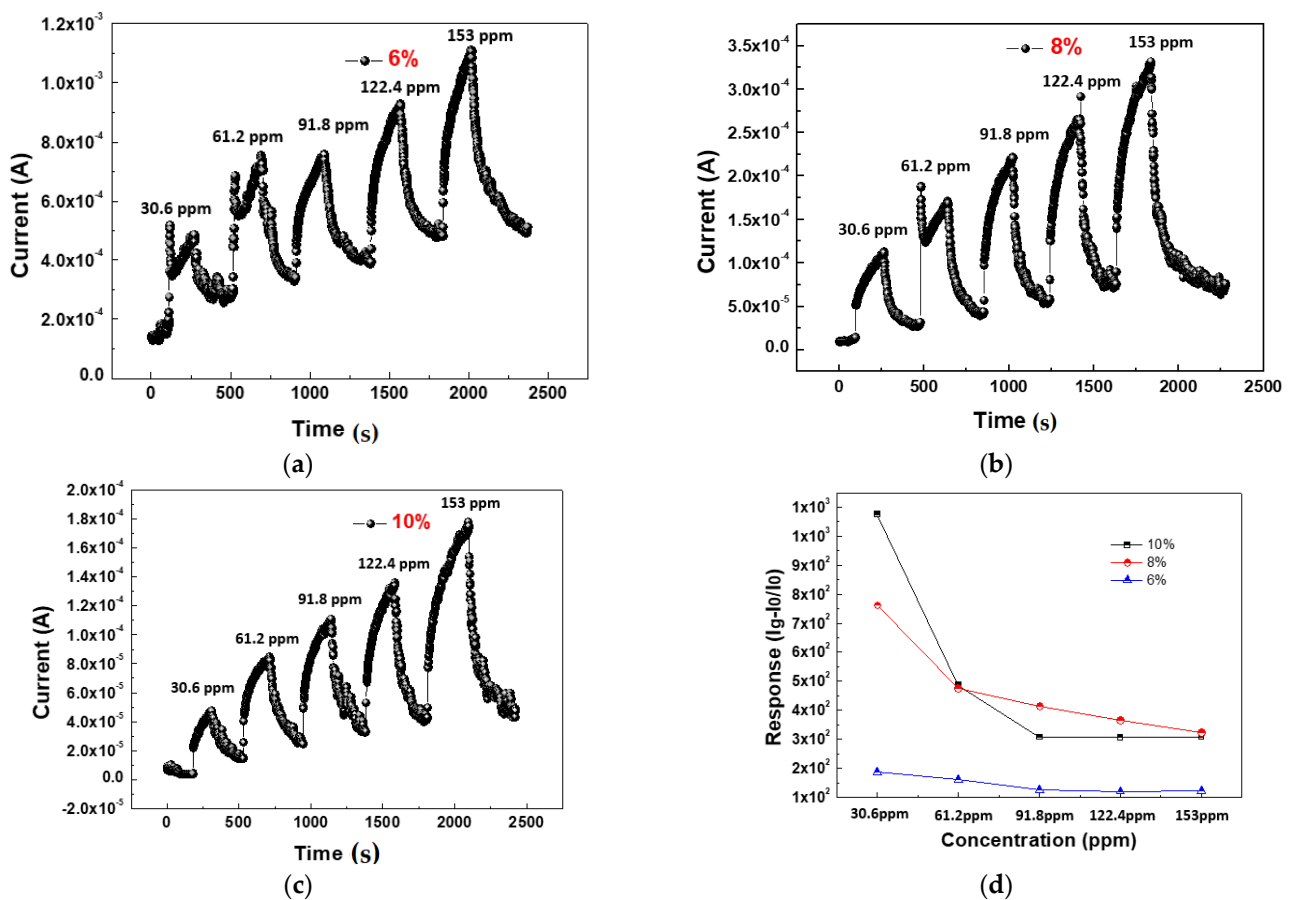


Figure 8. Sensing transients to SO₂ for samples with (a) 6%, (b) 8%, (c) 10% oxygen flow ratio at 300 °C; (d) the sensing response of three different oxygen ratios.

Table 1. Gas-sensing performance (%) of 6%, 8%, 10% samples (300 °C) as a function of sulfur dioxide (SO₂) concentration.

SO ₂ /Oxygen Flow	30.6 ppm	61.2 ppm	91.8 ppm	122.4 ppm	153 ppm
10%	1075	486	307	306	307
8%	762	475	415	365	323
6%	186	160	125	120	122

As seen in Figure 9b, the sensitivity was 0% without UV treatment at 150 °C. The temperature, which was below 250 °C, could not cause the oxygen ions species to be adsorbed on the sensing film's surface. However, the responsivity raised to 55% when the sample was measured under UV light irradiation. Based on the chemical adsorption, the oxygen ion traps and analyte gas reactions produced electrons, which caused the current increment. The working temperature of the InTiZnO gas sensor was around 250–400 °C, in which thermal energy could create a significant amount of oxygen ion traps. Electrons provided by UV irradiation also produced oxygen ion species on the InTiZnO surface. Therefore, the UV-activated traps could react with ethanol molecules and increase the current of the sensor.

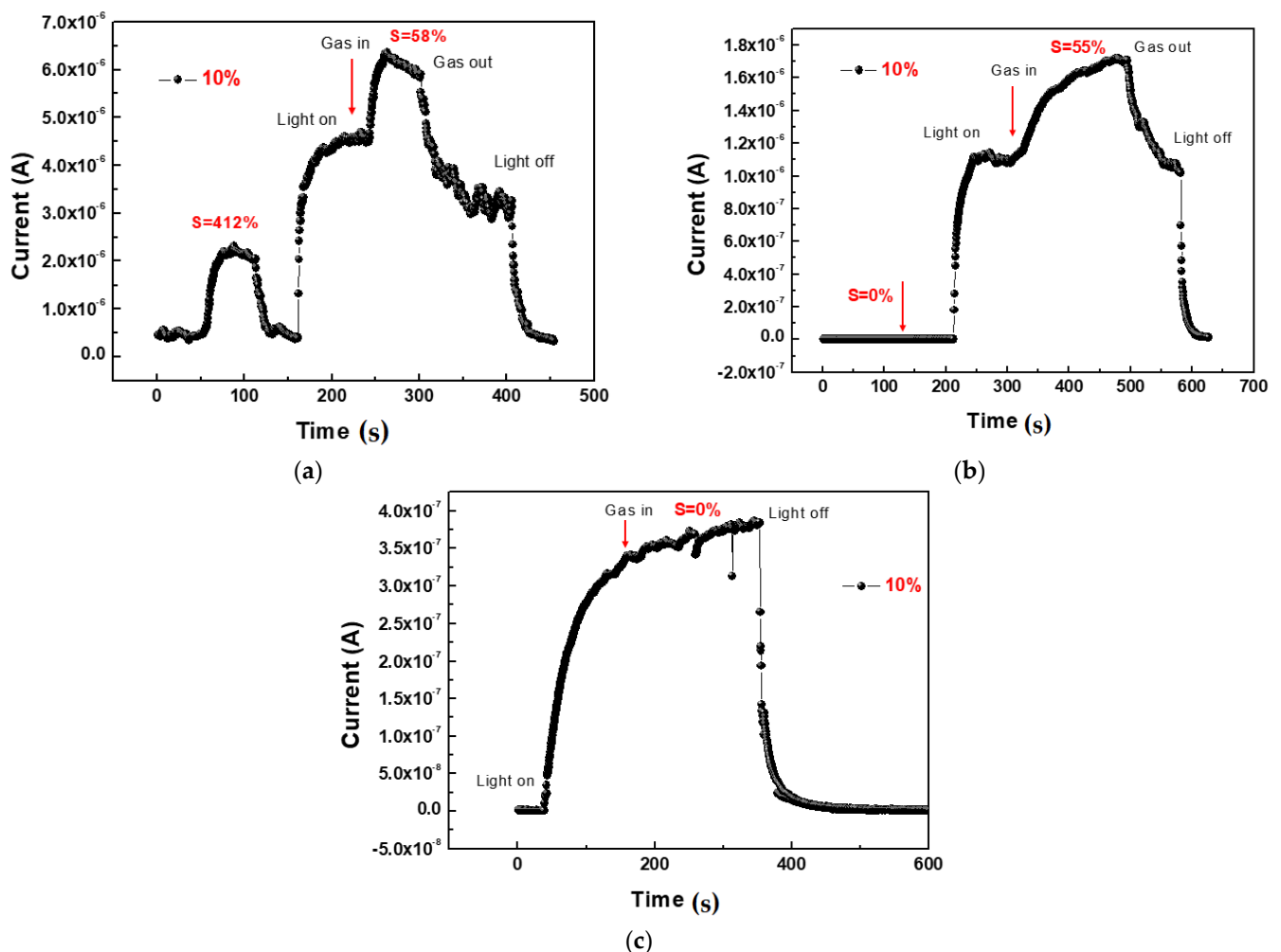


Figure 9. Current transient of 10% InTiZnO under 100 ppm ethanol at (a) 250 °C, (b) 150 °C, (c) 100 °C.

Figure 9c shows the transient response of the InTiZnO sensor to 100 ppm ethanol at 100 °C. It appears that there was no response observed before and after the UV light was turned on. Since the current was derived from the reaction of oxygen ion traps adsorbed at the surface, it was mainly given by temperature. When the sensor was measured at a relatively low temperature, the UV could not enhance the response compared to high-temperature conditions. UV irradiation energy was not enough to compensate for the decreased thermal energy.

4. Conclusions

In this research, an InTiZnO gas sensor with an MSM structure was fabricated. First, we analyzed films with different O₂/Ar ratios. When the O₂/Ar ratio increases, it will result in a more significant surface area to volume ratio and will adjust the oxygen vacancies in the film. Subsequently, we measured different gases at a measurement temperature of 300 °C. As O₂/Ar increases, the response to each gas also increases. The results show that the gas sensor has the best response and the best selectivity to alcohol when the oxygen ratio is 10%. In addition, the InTiZnO gas sensor activated by ultraviolet light was also studied. Since InTiZnO is sensitive to light, ultraviolet rays can cause electrons to be activated more easily, reducing the response temperature of the device, thereby improving the performance of the sensor. In summary, the high response and selectivity indicate that InTiZnO thin films have high application potential in gas sensing technology.

Author Contributions: S.-P.C. designed and performed the experiments, conceptualization, and methodology and analyzed the data. S.-P.C. and R.-H.Y. wrote the manuscript in consultation with C.-H.L. All authors have read and agreed to the published version of the manuscript.

Funding: This work was supported by the Ministry of Science and Technology under contract number MOST 107-2221-E-006-146 and 107-2221-E-006-189-MY3.

Institutional Review Board Statement: Not applicable.

Informed Consent Statement: Not applicable.

Data Availability Statement: Not applicable.

Acknowledgments: The authors gratefully acknowledge the use of JEOL JEM-2100F CS STEM equipment belonging to the Instrument Center of National Cheng Kung University.

Conflicts of Interest: The authors declare no conflict of interest.

References

1. Dey, A. Semiconductor metal oxide gas sensors: A review. *Mater. Sci. Eng. B Adv. Funct. Solid State Mater.* **2018**, *229*, 206–217. [[CrossRef](#)]
2. Korotcenkov, G. Metal oxides for solid-state gas sensors: What determines our choice? *Mater. Sci. Eng. B Solid State Mater. Adv. Technol.* **2007**, *139*, 1–23. [[CrossRef](#)]
3. Korotcenkov, G. The role of morphology and crystallographic structure of metal oxides in response of conductometric-type gas sensors. *Mater. Sci. Eng. R Rep.* **2008**, *61*, 1–39. [[CrossRef](#)]
4. Rieu, M.; Camara, M.; Tournier, G.; Viricelle, J.P.; Pijolat, C.; de Rooij, N.F.; Briand, D. Fully inkjet printed SnO₂ gas sensor on plastic substrate. *Sens. Actuator B Chem.* **2016**, *236*, 1091–1097. [[CrossRef](#)]
5. Zhu, L.; Zeng, W. Room-temperature gas sensing of ZnO-based gas sensor: A review. *Sens. Actuator A Phys.* **2017**, *267*, 242–261. [[CrossRef](#)]
6. Urasinska-Wojcik, B.; Vincent, T.A.; Chowdhury, M.F.; Gardner, J.W. Ultrasensitive WO₃ gas sensors for NO₂ detection in air and low oxygen environment. *Sens. Actuator B Chem.* **2017**, *239*, 1051–1059. [[CrossRef](#)]
7. Liu, Y.; Wang, L.; Wang, H.; Xiong, M.; Yang, T.; Zakharova, G.S. Highly sensitive and selective ammonia gas sensors based on PbS quantum dots/TiO₂ nanotube arrays at room temperature. *Sens. Actuator B Chem.* **2016**, *236*, 529–536. [[CrossRef](#)]
8. Afshar, M.; Preiß, E.M.; Sauerwald, T.; Rodner, M.; Feili, D.; Straub, M.; Seidel, H. Indium-tin-oxide single-nanowire gas sensor fabricated via laser writing and subsequent etching. *Sens. Actuator B Chem.* **2015**, *215*, 525–535. [[CrossRef](#)]
9. Behera, B.; Chandra, S. An innovative gas sensor incorporating ZnO-CuO nanoflakes in planar MEMS technology. *Sens. Actuator B Chem.* **2016**, *229*, 414–424. [[CrossRef](#)]
10. Lee, K.I.; Kim, E.K.; Kim, H.D.; Kang, H.I.; Song, J.T. Low temperature Al doped ZnO films on a flexible substrate by DC sputtering. *Phys. Status Solidi C* **2008**, *5*, 3344–3347. [[CrossRef](#)]
11. Minami, T. Transparent conducting oxide semiconductors for transparent electrodes. *Semicond. Sci. Technol.* **2005**, *20*, S35–S44. [[CrossRef](#)]
12. Nomura, K.; Kamiya, T.; Ohta, H.; Hirano, M.; Hosono, H. Defect passivation and homogenization of amorphous oxide thin-film transistor by wet O₂ annealing. *Appl. Phys. Lett.* **2008**, *93*, 192107. [[CrossRef](#)]
13. Liu, A.; Liu, G.X.; Shan, F.K.; Zhu, H.H.; Shin, B.C.; Lee, W.J.; Cho, C.R. High-performance InTiZnO thin-film transistors deposited by magnetron sputtering. *Chin. Phys. Lett.* **2013**, *30*, 127301. [[CrossRef](#)]
14. Majhi, S.M.; Mirzaei, A.; Kim, H.W.; Kim, S.S.; Kim, T.W. Recent advances in energy-saving chemiresistive gas sensors: A review. *Nano Energy* **2021**, *79*, 105369. [[CrossRef](#)] [[PubMed](#)]
15. Hsu, C.L.; Chang, L.F.; Hsueh, T.J. Light-activated humidity and gas sensing by ZnO nanowires grown on LED at room temperature. *Sens. Actuator B Chem.* **2017**, *249*, 265–277. [[CrossRef](#)]
16. Dhahri, R.; Hijiri, M.; Mir, L.E.; Banavita, A.; Iannazzo, D.; Latino, M.; Donato, N.; Neri, G. Gas sensing properties of Al-doped ZnO for UV-activated CO detection. *J. Phys. D Appl. Phys.* **2016**, *49*, 135502. [[CrossRef](#)]
17. Cheng, H.; Liu, Y.; Xie, C.S.; Wu, J.; Zheng, D.W.; Liao, Y.C. A comparative study on UV light activated porous TiO₂ and ZnO film sensors for gas sensing at room temperature. *Ceram. Int.* **2012**, *38*, 503–509. [[CrossRef](#)]
18. Gui, Y.; Li, S.; Xu, J.; Li, C. Study on TiO₂-doped ZnO thick film gas sensors enhanced by UV light at room temperature. *Microelectron. J.* **2008**, *39*, 1120–1125. [[CrossRef](#)]
19. Gong, J.; Li, T.; Zhai, X.; Hu, Z.; Deng, Y. UV-light-activated ZnO fibers for organic gas sensing at room temperature. *J. Phys. Chem. C* **2010**, *114*, 1293–1298. [[CrossRef](#)]
20. Hsueh, T.J.; Chang, S.J.H.; Hsu, C.L.; Lin, Y.R.; Chen, I.C. Highly sensitive ZnO nanowire ethanol sensor with Pd adsorption. *Appl. Phys. Lett.* **2007**, *91*, 053111. [[CrossRef](#)]
21. Hsueh, T.J.; Hsu, C.L.; Chang, S.J.; Chen, I.C. Laterally grown ZnO nanowire ethanol gas sensors. *Sens. Actuator B Chem.* **2007**, *126*, 473–477. [[CrossRef](#)]

-
22. Hsueh, T.J.; Chang, S.J.; Hsu, C.L.; Lin, Y.R.; Chen, I.C. ZnO nanotube ethanol gas sensors. *J. Electrochem. Soc.* **2008**, *155*, K152–K155. [[CrossRef](#)]
 23. Giessibl, F.J. Principle of NC-AFM. In *Noncontact Atomic Force Microscopy*; Springer: Berlin/Heidelberg, Germany, 2002; pp. 11–46.
 24. Wang, C.X.; Yin, L.W.; Zhang, L.Y.; Xiang, D.; Gao, R. Metal oxide gas sensors: Sensitivity and influencing factors. *Sensors* **2010**, *10*, 2088–2106. [[CrossRef](#)]